Reset control for active vibration isolation in the presence of wide-band disturbances

Berg, R.A.C. van den; Kaczmarek, M.B.; Natu, A.M.; HosseinNia, S.H.

DOI
10.1016/j.ifacol.2025.10.181

Publication date
2025

Document Version
Final published version

Published in
IFAC-PapersOnline

Available online at www.sciencedirect.com

ScienceDirect

IFAC Papers Online CONFERENCE PAPER ARCHIVE

IFAC PapersOnLine 59-17 (2025) 305–310

Reset control for active vibration isolation in the presence of wide-band disturbances ⋆

R.A.C. van den Berg * **M.B. Kaczmarek** * **A.M. Natu** * **S.H. HosseinNia** *

* *Department of Precision and Microsystems Engineering, Delft University of Technology, Mekelweg 2, 2628 CD Delft, The Netherlands (e-mail: A.M.Natu@tudelft.nl)*

Abstract: This paper explores the use of reset control in systems subjected to wide-band disturbances. Such excitation may result in too rare or excessive resetting, leading to deteriorated performance. Moreover, the commonly used Describing Function (DF) approximation for the frequency-domain design of reset systems does not sufficiently represent the reset element's behavior under such conditions as it is defined for sinusoidal excitation. To address this, we present a design approach based on analyzing the power spectral densities (PSD) of the signals in the system and using the Best Linear Approximations (BLA) of reset elements. In the first step, the dominant components in the PSD of the reset triggering signal are related to the frequency domain properties of the reset element. To benefit from resetting, it should lead to an increase in phase margins near the cross-over frequency. This is the case where the components at the cross-over frequency dominate the reset triggering signal. To ensure this, the use of a bandpass shaping filter is proposed. In the second step, the BLA of the reset element is used to represent its response to the signal with a specific PSD in the frequency domain. This information is used to tune both the reset element and the shaping filter to achieve the desired performance and minimize loss of gain at low frequencies. Closed-loop simulations show the method's feasibility in achieving the desired behavior of the reset element, leading to improved resonance peak damping in the example studied.

Keywords: Reset Control, Disturbance Rejection, Best Linear Approximation (BLA), Wideband Noise, Bandpass, Shaping Filter

1. INTRODUCTION

Reset control systems are emerging as an augmentation for linear control, making it possible to overcome the inherent limitations related to the waterbed effect and the Bode gain-phase relationship, which has been shown in multiple studies, especially in the field of precision motion control. Depending on the controller design, an improved transient response, steady-state tracking of reference signals, or disturbance rejection can be achieved (Caporale et al. (2024)).

The benefits of the reset action can be clearly presented using the Describing Function (DF) approximation, such as the reduction of the phase lag of the integrator by 52° (Guo et al. (2009)). This advantage is clearly visible in the "Constant-in-Gain, Lead-in-Phase" (CgLp) element introduced by Saikumar et al. (2019), which, based on DF analysis, can provide phase lead while maintaining constant gain at a selected range of frequencies. This property can be used to increase the phase margins of control systems, leading to performance improvements.

Reset control systems can be designed using loop shaping in a procedure analogous to the design of commonly employed PID controllers (Saikumar et al. (2021)), making them suitable for wide adoption in the industry. The most popular frequency domain design methods for reset systems are based on sinusoidal input describing functions (Nuij et al. (2006)). However, since the reset systems are non-linear and the superposition principle does not apply, these methods cannot capture the system's behavior in the presence of wide-frequency band disturbances. Such disturbances may originate from the system's surroundings (e.g., floor vibrations) resulting from noisy signals used for control or parasitic dynamics in the system. Wide-band excitation may lead to too rare or excessive resetting. In both cases, the behavior of the reset control system is different from that expected based on DF, and its benefits are not observed. This poses a challenge in the design of reset systems for many real-life applications.

This paper presents an approach to the design of reset control systems for applications with wideband excitations. First, the PSD or a reset triggering signal is analyzed, and the dominant frequencies are related to the reset action. The behavior of the reset element in the presence of a signal with a specific PSD is represented in the frequency domain using the Best Linear Approximation (BLA). To ensure that the response of the reset element and the response of a closed-loop reset system follow the predictions of the DF, a method to tune the shaping filters is

⋆ This work was supported by the NWO HTSM Applied and Technical Science Program under project MetaMech with number 17976.

10.1016/j.ifacol.2025.10.181

proposed. The validity of the approach is illustrated with simulations.

The structure of the paper is as follows. In Section 2, the preliminaries of the reset control and the BLA are given. Section 3 presents the design of a linear and reset controller for active vibration isolation in an example introducing the problem. The analysis of the PSD of the reset triggering signal is provided in Section 4. The open-loop behavior of a FORE subjected to wideband noise is studied in Section 5. The results of closed-loop simulations are presented in Section 6. Lastly, the conclusions of this paper are given in Section 7.

2. PRELIMINARIES

This section presents the studied class of reset systems and their commonly used frequency-domain approximations. Moreover, we present the Best Linear Approximations of non-linear systems, which will be used as a new design tool for rest control systems.

2.1 Reset systems

The state-space representation of the reset element is

$$R:\begin{cases}\dot{x}_r(t) = A_r x_r(t) + B_r u_r(t), & \rho(t) \neq 0,\\ x_r(t^+) = A_\rho x_r(t), & \rho(t) = 0\\ y_r(t) = C_r x_r(t) + D_r u_r(t),\end{cases}, \tag{1}$$

where $x_r \in \mathbb{R}^{n_r}$ is the state of R, $x_r(t^+) = x_r^+ = \lim_{\epsilon\to 0^+} x(t+\epsilon)$ is the value of the state after reset, $u_r \in \mathbb{R}^m$ is the input of R, $y_r \in \mathbb{R}^m$ is the output of R andA_r, B_r, A_ρ, C_r, D_r are constant matrices of appropriate dimensions.

The base linear system (BLS) R_{bls} is an LTI system with a state-space realization

$$(A_r, B_r, C_r, D_r), \tag{2}$$

and describes the dynamics of R in the absence of reset. The reset is triggered by a signal $\rho(t)$. The linear reset law $x_r^+ = A_\rho x_r(t)$ describes the state change that occurs in the reset instants $t_k, k = 1, 2, \ldots$, that is, when the reset condition $\rho = 0$ is satisfied.

A specific type of reset element that is of concern in the paper is the First Order Reset Element (FORE), represented by (1) with

$$A_r = -\omega_r, \quad B_r = \omega_r, \quad C_r = 1, \quad D_r = 0, \quad A_\rho = \gamma,$$

where ω_r denotes the corner frequency of the element and $\gamma \in [-1, 1]$. In the manipulations of the transfer function, the elements can be represented by $\frac{1}{s/\omega_r+1}\nearrow^{\gamma}$, where the arrow indicates the resetting action.

2.2 Describing function representation

The Higher-Order Sinusoidal Input Describing Function (HOSIDF) Nuij et al. (2006) is a quasi-linearization of a nonlinear element that considers its steady-state response to a sinusoidal excitation. The non-linear element is considered as a virtual harmonic generator, and HOSIDF of nth order is defined

$$H_n(j\omega) = \frac{a_n(\omega)e^{j\phi_n(a_0,\omega)}}{a_0}, \tag{3}$$

where a_n and ϕ_n denote the nth component of the Fourier series expansion of the steady-state output of the element for a sinusoidal input.

The first-order HOSIDF (DF) of an open-loop reset element has been derived in Guo et al. (2009), and the higher-order components were presented in Saikumar et al. (2021). In Dastjerdi et al. (2023), the HOSIDF for a closed-loop system with a reset controller was introduced, and the calculations necessary for the HOSIDF analysis of reset systems were implemented in the form of a user-friendly Matlab toolbox.

2.3 CgLp

Constant-in-Gain, Lead-in-Phase (CgLp) introduced by Saikumar et al. (2019) consists of a reset lag element in series with a linear lead filter. In the FORE-based version

$$R = \frac{1}{s/\omega_r+1}\nearrow^{\gamma}, \qquad D(s) = \frac{s/\omega_{r,\alpha}+1}{s/\omega_f+1}, \tag{4}$$

where the corner frequency of the lead filters $\omega_{r,\alpha} = \alpha\omega_r, \alpha \in \mathbb{R}$ is adjusted to account for a shift in corner frequency of the lag filter due to resetting action.

The phase lead in the frequency range (ω_r, ω_f) is obtained using the reduced phase lag of the reset lag element (when the first harmonic of HOSIDF is considered) combined with a corresponding lead element. Ideally, the gain of the reset lag element should be canceled out by the gain of the corresponding linear lead element, which creates a constant gain behavior.

2.4 Best linear approximation of a non-linear system

The Best Linear Approximation (BLA) is based on the idea that a nonlinear system can be represented by a combination of an LTI model and non-linear disturbance, both of which depend on the power spectrum of the input signal. The BLA can be obtained nonparametrically by performing classical frequency response function (FRF) measurements

$$G_{BLA}(j\omega_k) = \frac{S_{yu}(j\omega_k)}{S_{uu}(j\omega_k)}, \tag{5}$$

where $S_{yu}(j\omega_k)$ is the cross-power spectrum between the output y and the input u of the system, and $S_{uu}(j\omega_k)$ is the auto-power spectrum of the input (Pintelon and Schoukens (2012)). The BLA can also be measured in closed-loop systems (Pintelon et al. (2020)), including noise and disturbance signals.

3. PROBLEM DESCRIPTION

This section presents the problem under study, including the control structure used and the challenges related to implementing reset control in systems with wideband disturbances.

3.1 Plant

Consider a vibration isolation system presented in Fig. 1, consisting of a mass to be isolated with position x_2 on a shaking base with x_1. In this work, we focus on reducing

the influence of the base vibration $\ddot{x}_1$ (with a PSD specified in Spanjer and Hakvoort (2022)) on the acceleration $\ddot{x}_2$ of the isolated mass using a feedback controller.

The dynamics of the plant are captured by the transmissibility

$$P_t(s) = \frac{\ddot{x}_2(s)}{\ddot{x}_1(s)} = \frac{1}{\frac{s^2}{\omega_p^2} + 2\zeta\frac{s}{\omega_p} + 1}, \tag{6}$$

and compliance

$$P_c(s) = \frac{\ddot{x}_2(s)}{F_d(s)} = \frac{s^2/k}{\frac{s^2}{\omega_p^2} + 2\zeta\frac{s}{\omega_p} + 1}, \tag{7}$$

with $\omega_p = 104$ Hz denoting the resonance frequency, stiffness $k = 2.39 \cdot 10^7$ N·m/s, damping ratio of the plant $\zeta_p = 0.0022$. In the design of the feedback system, a delay $\tau = 0.7$ ms should also be included.

The control loop comprises the reset element R and the LTI control block C_L. The behavior of the system can also be influenced by placing a linear shaping filter $C_{SF}(s)$ on the reset triggering signal ρ (Karbasizadeh et al. (2020a)). The influence of the measurement noise n and direct disturbance forces F_d are considered negligible in the analysis of the system.

3.2 LTI Controller design

To dampen the resonance peak of the plant, the Linear Time-Invariant (LTI) controller employs Direct Velocity Feedback (DVF)(Balas (1979)). Since acceleration is measured as an output of the plant, the DVF has a transfer function

$$C_v(s) = \frac{K_v}{s + \omega_v}, \tag{8}$$

and its parameters are presented in Tab. 1. Such a controller results in a triangular loop gain $C_v(s)P_c(s)$ presented in Fig. 2a with crossover frequencies $\omega_{c,1}$ and $\omega_{c,2}$, at which $|C_v(\omega_{c,2})P_c(\omega_{c,2})| = 1$. These crossover frequencies and the corresponding phase margins are key to the stability and performance of the system. The maximum gain of the controller K_v resulting in 30° phase margin at the second crossover frequency is selected. The achievable gain is limited by the phase loss due to the time-delay in the system.

Table 1. Parameters of the controllers, where the BLS also functions as the linear part of the reset controller.

	K_v	ω_v [Hz]	$\omega_{c,2}$ [Hz]	PM [°]
LTI	$7.2 \cdot 10^4$	5	248	30
BLS	$1 \cdot 10^5$	5	313	12

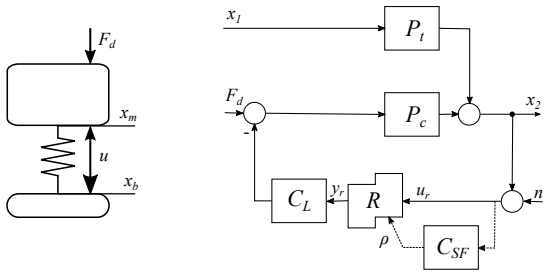

Fig. 1. Closed-loop diagram of a reset control system for AVC

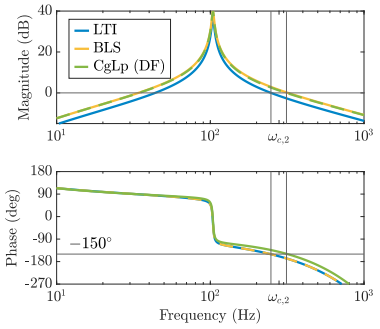

(a)

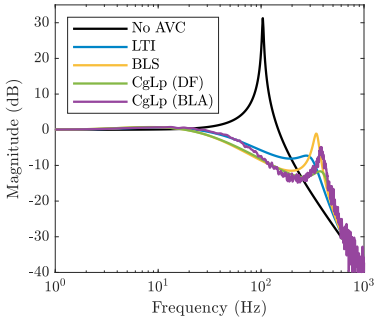

(b)

Fig. 2. (a) Open-loop with the different controllers. An optimal shape is a triangular shape centered at the resonance frequency. Second crossover frequency $\omega_{c,2}$ is indicated with the vertical line, for both the LTI and BLS controller. (b) Transmissibility from x_1 to x_2 of the system with no AVC and with different strategies implemented, showing the improvement in disturbance rejection performance. The BLA highlights the deteriorated performance under wideband noise conditions.

3.3 Reset Controller design

Increasing the controller gain while maintaining the desired phase margins would lead to a stronger reduction of the system's transmissibility without sacrificing stability. A CgLp element is introduced into the control structure to make this possible. In this example, the liner controller with an increased gain has a phase margin at $\omega_{c,2}$ of only 12°, indicated with Base Linear System (BLS) in Fig. 2a. The CgLp element provides an additional 18° of phase lead (analyzed with DF), resulting in the same combined value as in the LTI system.

The desired amount of phase provided by the CgLp element can be achieved with different combinations of parameter values. In this first example, the element was constructed with $\omega_r = 150$ Hz, $\omega_f = 10$ kHz, $\alpha = 1.62$ and $\gamma = 0$. Referring to the control structure in Fig. 1, non-linear element R is equal to the FORE part of CgLp and

$$C_{SF}(s) = 1, \qquad C_L(s) = C_v(s)D(s),$$

where C_L consists of the lead part of the CgLp (4) and the DVF (8). The parameters of the controller are presented in Tab. 1 under BLS.

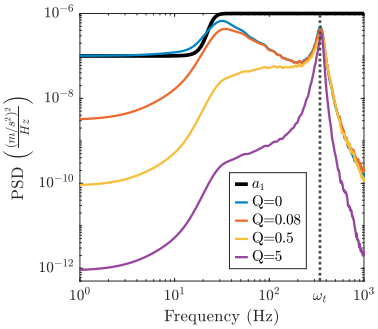

Fig. 3. PSD of floor disturbance profile a_1 and PSD of the reset triggering signal ρ in closed-loop simulation for different widths Q of the BPF. The dotted line denotes the closed-loop resonance frequency, $\omega_t = 343$Hz.

3.4 Problem identification

The closed-loop transmissibility between $\ddot{x}_1$ and $\ddot{x}_2$ of the system is presented in Fig. 2b. The DF approximation of the reset system suggests a stronger disturbance rejection than in the LTI case without creating an excessive resonance peak close to $\omega_{c,2}$. However, when a time simulation of the rest system is performed, the resulting BLA shows a significant resonance peak. This suggests that the reset system is not effective. The DF-based analysis of a reset element assumes a single sinusoidal excitation and cannot capture the behavior of a reset system excited by a signal with an arbitrary power spectrum. This is due to the fact that the superposition principle does not apply. In the remainder of the paper, we show a design strategy to achieve the desired performance.

4. PSD OF THE RESET TRIGGERING SIGNAL IN CLOSED-LOOP

The sequence of reset instances for a system excited by a multi-harmonic signal is not merely the sum of the reset instances caused by each harmonic independently. Figure 3 presents the Power Spectral Density (PSD) of the reset triggering signal ρ in the closed-loop simulation, along with the PSD of the floor excitation signal used. In the case studied in the previous section ($Q = 0$), the reset triggering signal contains a wide range of frequencies. It is dominated by low-frequency components with a smaller peak around the second crossover frequency. Such a spectrum indicates a complicated reset sequence, as multiple components with similar amplitudes and different frequencies constitute the signal.

To benefit from the properties of the CgLp element, it must provide a phase lead at a desired frequency, in this case around $\omega_{c,2}$. To ensure this, we propose to make a single frequency dominant in the reset triggering signal by adding a shaping filter

$$C_{SF}(s) = \frac{\frac{\omega_c}{Q}s}{s^2 + \frac{\omega_c}{Q}s + \omega_c^2}, \tag{9}$$

with $|C_{SF}(j\omega_c| = 1$ at the center frequency ω_c. The width of the filter is determined by the value of Q, with a larger value resulting in a narrower filter.

Fig. 3 shows the effect of shaping ρ with different bandpass filter (BPF) widths on S_ρ in closed-loop. As the BPF narrows, the target frequency ω_t becomes more dominant in the reset triggering signal because the magnitude of the low-frequency content becomes smaller. This should enable benefiting from reset in the desired frequency range.

5. OPEN-LOOP BEHAVIOR OF A FORE IN THE PRESENCE OF WIDEBAND DISTURBANCES

Before showing the actual BLA of a reset system with wideband input signals, we present a time-domain illustration of a reset element's behavior in Fig. 4. In the figure, we study different cases of the response of a reset element with a single sinusoidal input signal u_r with frequency ω_{u_r}. In each case, the resets are forced by a signal ρ with a different frequency ω_ρ.

The standard case, considered in the DF analysis, is presented in Fig. 4b. The reset is triggered by ρ, which has the same frequency as the input signal u_r.

Excessive resetting is illustrated in Fig. 4a, where the resetting frequency is much higher than the input signal frequency. In such a case, the magnitudes of the FORE's response decrease, as there is not enough time for the response to rise to the values obtained by the BLS of the element. The extent of the magnitude decreases is related to the corner frequency of the element, ω_r, in a similar way to which it defines the speed of the step response for linear systems.

When the resetting frequency is much lower than the input frequency, the resetting action has a minor influence on the system behavior, as illustrated in Fig. 4c. In such a case, the response of the reset element should closely match that of its BLS, and no advantage of the reset element will be exhibited in the frequency domain.

The BLA captures the behavior of a reset element with an input signal with a specific PSD in the frequency domain. In Fig. 5, the BLA of FORE in an open-loop with and without band-pass filters is presented. The FORE parameters are $\omega_r = 380$ Hz, $\alpha = 1.11$, and $\gamma = 0.4$. The input signal u_r of FORE is obtained from a closed-loop simulation without a shaping filter. In an open-loop simulation, the reset triggering signals pass through filters of various widths Q. In each case, the BLA is calculated between the input and the output of the FORE. The BLA is compared with the FORE DF, which has the same parameters but without the shaping filer.

At low frequencies, the BLA for all filter widths exhibits a smaller magnitude when compared to the DF. This behavior is related to excessive resetting, similar to the case presented in Fig. 4a. Resets are triggered with high frequency, related to the dominant components of ρ presented in Fig. 3. When narrower band-pass filters are used, the components of ρ near the closed-loop resonance frequency ω_t become more dominant, and stronger gain loss at low frequencies can be seen in the BLA.

The BLA of the reset system matches the DF only within the frequency range close to the frequency of the reset triggering signal. Fig. 5b highlights the BLA of FORE near the closed-loop resonance frequency ω_t. Selecting a

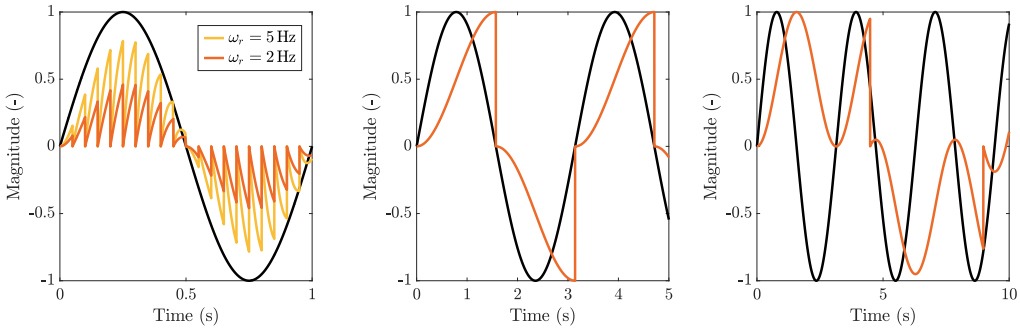

(a) $\omega_\rho >> \omega_{u_r}$ (b) $\omega_\rho = \omega_{u_r}$ (c) $\omega_\rho << \omega_{u_r}$

Fig. 4. Simplified time-domain illustration of the behavior of a reset system, when input frequency ω_{u_r} and the reset frequency ω_ρ are not necessarily the same. The input (black) is a single sine wave. a) Resetting too fast. Depending on ω_r of FORE being closer to ω_ρ, the gain of the output is closer to its input. b) Standard situation for a Clegg Integrator. Resets take place with the input frequency. c) Clegg Integrator with slow resetting.

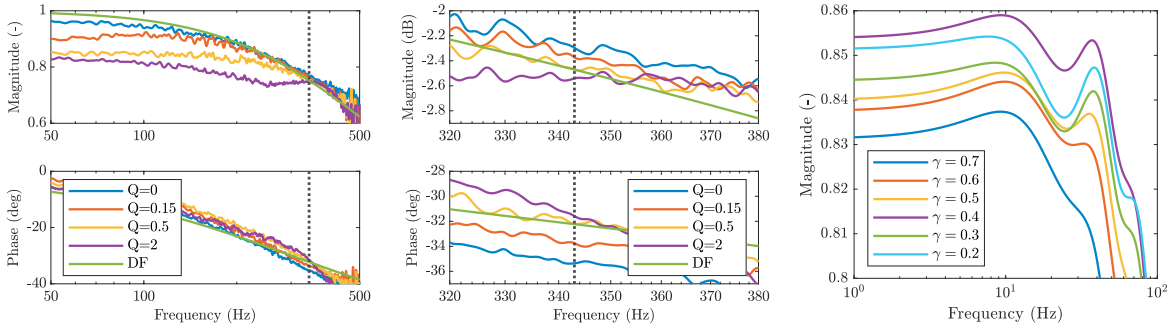

(a) Filter width Q (b) Filter width Q, zoom-in (c) Partial reset γ

Fig. 5. a) BLA between y_r in open-loop for different BPF widths and u_r in closed-loop without BPF, compared to DF of FORE. b) presents the crossover region in detail. The closed-loop resonance frequency is indicated with the dotted line, which is the desired frequency for matching. c) BLA of FORE in open-loop for different values of γ. The corresponding value of ω_r is maximized to reduce gain loss.

band-pass filter with $Q = 0.5$ results in the closest match between the BLA and DF of the element at the target frequency. The rigorous explanation for why this is the case should be a subject of future study.

At high frequencies, above the resonance frequency ω_t, the response of the reset element is dominated by the higher harmonics of the reset frequency, which are represented by spikes in the BLA, which are not shown in the figure for clarity. This is related to the higher-order harmonics of the reset systems, and several strategies are available to reduce this effect, presented by Karbasizadeh et al. (2020b,a) and Karbasizadeh and HosseinNia (2022).

To minimize the loss of low-frequency gain, the maximum possible value of ω_r should be selected, as suggested by Fig. 4a. Fig. 5c compares the FORE BLA with different combinations of ω_r and γ, leading to the same phase lead in the DF at ω_t. Selecting γ closer to 0 leads to stronger resets, and the same phase lead can be achieved with a narrower CgLp. Although the differences are small, it can be seen that with $\gamma = 0.4$, the gain loss in the low-frequency region is minimized. Explicitly explaining why this combination of values leads to the best results should be further studied.

The results presented above indicate the trade-off between the phase provided by CgLp and the gain loss at lower frequencies. For given γ, the CgLp designed for a larger phase lead at the target frequency should be wider, requiring smaller ω_r. Lower ω_r leads to larger gain loss, leading to deterioration of system performance.

The CgLp for closed-loop simulations is designed with only 5° phase lead, limiting gain loss and still providing damping of the BLS resonance peak. The corresponding corner frequency is $\omega_r = 380$ Hz. The maximum possible ω_f, limited by the Nyquist frequency, is selected such that it has minimal influence on the phase lead at ω_t. For the shaping filter, a bandpass filter with $Q = 0.5$ is selected as it results in a close match between the BLA and the DF at the frequency of interest, as indicated in Fig. 5b.

6. CLOSED-LOOP TRANSMISSIBILITY ANALYSIS

In Fig. 6, the transmissibility relationships from closed-loop simulations with different controllers are compared with the prediction based on DF. In the absence of a shaping filter ($Q = 0$), the transmissibility BLA matches the DF closely at low frequency. However, the resonance

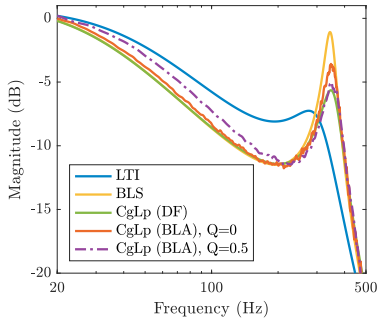

Fig. 6. Closed-loop transmissibility for different controller designs. DF-based vs. BLA for no BPF and BPF with $Q = 0.5$

peak close to ω_t is higher than expected, which corresponds to the lesser phase provided by the element (Fig. 5b).

Shaping the reset triggering signal with the tuned band-pass filter ($Q = 0.5$) results in a stronger reduction of the resonance peak and a close match to the prediction of DF around the resonance peak. This is at the cost of an increase in transmissibility at low frequency compared to the DF, due to the magnitude loss of FORE in that range of frequencies.

Both the magnitude loss and damping can be well explained using the BLA of the FORE from the open-loop simulation. At the same time, an accurate prediction of the closed-loop results, based on the open-loop BLA of a reset element, remains challenging. Modifying the reset element influences the PSD of the reset triggering signal. Improved damping due to the better design of the reset element will reduce the magnitude of the response in the target frequency range, possibly increasing the influence of the components in other frequencies on the reset sequence. Moreover, due to the non-linearity, the dynamics of a reset element is not fully captured by a BLA. However, in the presented case, the use of open-loop BLA estimations provided valuable information for designing an improved system.

7. DISCUSSION AND CONCLUSIONS

This paper studied the use of reset systems in the presence of wide-band excitations. To benefit from the reset element, the components at the cross-over frequency should dominate the reset triggering signal. To ensure this, a band-pass shaping filter was implemented. Forcing the resetting at a specific frequency has an influence on other frequency ranges, which can be represented by a BLA of a reset element. At lower frequencies, the gain of the element decreases, which can be mitigated to some extent by adjusting the parameters of the shaping filter and the reset element. The resetting frequency's harmonics dominate the element's response at higher frequencies.

REFERENCES

Balas, M.J. (1979). Direct Velocity Feedback Control of Large Space Structures. *Journal of Guidance and Control*, 2(3), 252–253. doi:10.2514/3.55869.

Caporale, D., van Eijk, L.F., Karbasizadeh, N., Beer, S., Kostic, D., and HosseinNia, S.H. (2024). Practical Implementation of a Reset Controller to Improve Performance of an Industrial Motion Stage. *IEEE Transactions on Control Systems Technology*, PP, 1–12. doi: 10.1109/TCST.2024.3374155.

Dastjerdi, A.A., Astolfi, A., Saikumar, N., Karbasizadeh, N., Valerio, D., and Hosseinnia, S.H. (2023). Closed-Loop Frequency Analysis of Reset Control Systems. *IEEE Transactions on Automatic Control*, 68(2), 1146–1153. doi:10.1109/TAC.2022.3184039.

Guo, Y., Wang, Y., and Xie, L. (2009). Frequency-domain properties of reset systems with application in hard-disk-drive systems. *IEEE Transactions on Control Systems Technology*, 17(6), 1446–1453. doi: 10.1109/TCST.2008.2009066.

Karbasizadeh, N., Dastjerdi, A.A., Saikumar, N., and HosseinNia, S.H. (2020a). Band-Passing Nonlinearity in Reset Elements.

Karbasizadeh, N., Dastjerdi, A.A., Saikumar, N., Valerio, D., and Hossein Nia, S.H. (2020b). Benefiting from linear behaviour of a nonlinear reset-based element at certain frequencies. In *2020 Australian and New Zealand Control Conference, ANZCC 2020*, 226–231. Institute of Electrical and Electronics Engineers Inc. doi:10.1109/ANZCC50923.2020.9318363.

Karbasizadeh, N. and HosseinNia, S.H. (2022). Continuous reset element: Transient and steady-state analysis for precision motion systems. *Control Engineering Practice*, 126, 105232. doi:10.1016/j.conengprac.2022.105232.

Nuij, P.W.J.M., Bosgra, O.H., and Steinbuch, M. (2006). Higher-order sinusoidal input describing functions for the analysis of non-linear systems with harmonic responses. *Mechanical Systems and Signal Processing*, 20, 1883–1904. doi:10.1016/j.ymssp.2005.04.006.

Pintelon, R. and Schoukens, J. (2012). System Identification: A Frequency Domain Approach. In *Encyclopedia of Systems and Control*, 469–479. URL `https://ieeexplore.ieee.org/book/6198969`.

Pintelon, R., Schoukens, M., and Lataire, J. (2020). Best Linear Approximation of Nonlinear Continuous-Time Systems Subject to Process Noise and Operating in Feedback. *IEEE Transactions on Instrumentation and Measurement*, 69(10), 8600–8612. doi: 10.1109/TIM.2020.2987476.

Saikumar, N., Heinen, K., and HosseinNia, S.H. (2021). Loop-shaping for reset control systems: A higher-order sinusoidal-input describing functions approach. *Control Engineering Practice*, 111, 104808. doi: 10.1016/J.CONENGPRAC.2021.104808.

Saikumar, N., Sinha, R.K., and Hassan Hosseinnia, S. (2019). 'Constant in Gain Lead in Phase' Element-Application in Precision Motion Control. *IEEE/ASME Transactions on Mechatronics*, 24(3), 1176–1185. doi: 10.1109/TMECH.2019.2909082.

Spanjer, S.T. and Hakvoort, W.B. (2022). Optimal Active Vibration Isolation System Design using Constrained H2control. In *IFAC-PapersOnLine*, volume 55, 160–165. Elsevier. doi:10.1016/j.ifacol.2022.10.505.